Chapter Seventeen

Collisional Excitation

Collisional excitation is important in the ISM for two reasons:

1. It puts ions, atoms, and molecules into excited states from which they may decay radiatively; these radiative losses result in cooling of the gas.

2. It puts species into excited states that can serve as diagnostics of the physical conditions in the gas. If the level populations can be determined observationally, from either emission lines or absorption lines, we may be able to infer the density, temperature, or radiation field in the region where the diagnostic species is located.

Throughout this chapter and the rest of the book, we will be making use of rate coefficients and transition rates. We will use the notation $k_{if} \equiv \langle \sigma v \rangle_{i \to f}$ for collisional rate coefficients, and $A_{if} \equiv A_{i \to f}$ to denote radiative transition probabilities, where the first subscript in k_{if} or A_{if} denotes the initial state, and the second the final state. For energy-level differences, we will set $E_{u\ell} \equiv E_u - E_\ell$.

17.1 Two-Level Atom

In some cases, it is sufficient to consider only the ground state and the first excited state – when attention is limited to these two states, we speak of the "two-level atom." Consider first the case where there is no background radiation present, and the only processes acting are collisional excitation, collisional deexcitation, and radiative decay. Let the ground state be level 0, and the excited state be level 1. Let n_j be the number density of the species in level j. For collisional excitation by some species (e.g., electrons) with density n_c, the population of the excited state must satisfy

$$\frac{dn_1}{dt} = n_c n_0 k_{01} - n_c n_1 k_{10} - n_1 A_{10} \quad . \tag{17.1}$$

The steady state solution ($dn_1/dt = 0$) is simply

$$\frac{n_1}{n_0} = \frac{n_c k_{01}}{n_c k_{10} + A_{10}} \quad . \tag{17.2}$$

The upward rate coefficient k_{01} is given in terms of the downward rate coefficient

by

$$k_{01} = \frac{g_1}{g_0}\, k_{10}\, \mathrm{e}^{-E_{10}/kT_{\rm gas}} \quad , \tag{17.3}$$

where g_0, g_1 are the level degeneracies, and $T_{\rm gas}$ is the kinetic temperature of the gas. In the limit $n_c \to \infty$, it is easy to see that $n_1/n_0 \to (g_1/g_0)\exp(-E_{10}/kT_{\rm gas})$.

Now suppose that radiation is present. Let u_ν be the specific energy density at frequencies near $\nu = E_{10}/h$. It is convenient to use instead the dimensionless (angle- and polarization-averaged) photon occupation number:

$$\bar{n}_\gamma \equiv \frac{c^3}{8\pi h\nu^3}\, u_\nu \quad . \tag{17.4}$$

Then,

$$\frac{dn_1}{dt} = n_0 \left[n_c k_{01} + \bar{n}_\gamma \frac{g_1}{g_0} A_{10} \right] - n_1 \left[n_c k_{10} + (1+\bar{n}_\gamma)\, A_{10} \right] \quad . \tag{17.5}$$

The rate of photoabsorption is $\bar{n}_\gamma (g_1/g_0) A_{10} n_0$, and the rate of stimulated emission is $\bar{n}_\gamma A_{10} n_1$ (see Chapter 6). The **steady-state solution with radiation present** is

$$\frac{n_1}{n_0} = \frac{n_c k_{01} + \bar{n}_\gamma (g_1/g_0) A_{10}}{n_c k_{10} + (1+\bar{n}_\gamma) A_{10}} \quad . \tag{17.6}$$

This is the fully general result for a two-level system.

It is instructive to examine Eq. (17.6) in various limits:

- If $\bar{n}_\gamma \to 0$, then we recover our previous result (17.2).
- If $n_c \to 0$, then $n_1/n_0 \to (g_1/g_0)\bar{n}_\gamma/(1+\bar{n}_\gamma)$. If we have a blackbody radiation field with temperature $T_{\rm rad}$ [i.e., $n_\gamma = 1/(\mathrm{e}^{E_{10}/kT_{\rm rad}} - 1)$], then $n_1/n_0 = (g_1/g_0)\mathrm{e}^{-E_{10}/kT_{\rm rad}}$.
- If we have a blackbody radiation field with temperature $T_{\rm rad} = T_{\rm gas}$, then $n_1/n_0 = (g_1/g_0)\mathrm{e}^{-E_{10}/kT_{\rm rad}}$ *independent* of the gas density n_c! The photons alone are sufficient to bring the two level system into LTE, and additional (thermal) collisions have no further effect on the level populations.

17.2 Critical Density $n_{\mathbf{crit},u}$

For a collision partner c, we define the **critical density** $n_{{\rm crit},u}(c)$ for an excited state u to be the density for which collisional deexcitation equals radiative deexcitation,

Table 17.1 Critical Densities for Fine-Structure Excitation in H I Regions

						$n_{\rm H,crit}(u)$	
			E_ℓ/k	E_u/k	$\lambda_{u\ell}$	$T = 100\,{\rm K}$	$T = 5000\,{\rm K}$
Ion	ℓ	u	(K)	(K)	(μm)	($\rm cm^{-3}$)	($\rm cm^{-3}$)
C II	$^2{\rm P}^{\rm o}_{1/2}$	$^2{\rm P}^{\rm o}_{3/2}$	0	91.21	157.74	2.0×10^3	1.5×10^3
C I	$^3{\rm P}_0$	$^3{\rm P}_1$	0	23.60	609.7	620	160
	$^3{\rm P}_1$	$^3{\rm P}_2$	23.60	62.44	370.37	720	150
O I	$^3{\rm P}_2$	$^3{\rm P}_1$	0	227.71	63.185	2.5×10^5	4.9×10^4
	$^3{\rm P}_1$	$^3{\rm P}_0$	227.71	326.57	145.53	2.3×10^4	8.4×10^3
Si II	$^2{\rm P}^{\rm o}_{1/2}$	$^2{\rm P}^{\rm o}_{3/2}$	0	413.28	34.814	1.0×10^5	1.1×10^4
Si I	$^3{\rm P}_0$	$^3{\rm P}_1$	0	110.95	129.68	4.8×10^4	2.7×10^4
	$^3{\rm P}_1$	$^3{\rm P}_2$	110.95	321.07	68.473	9.9×10^4	3.5×10^4

including stimulated emission[1]:

$$n_{{\rm crit},u}(c) \equiv \frac{\sum_{\ell<u}\left[1 + (n_\gamma)_{u\ell}\right] A_{u\ell}}{\sum_{\ell<u} k_{u\ell}(c)} \quad . \tag{17.7}$$

Note that the definition (17.7) applies to multilevel systems, but each excited level u may have a different critical density. The definition (17.7) is appropriate when the gas is optically thin, so that the radiated photons can escape. When the emitting gas is itself optically thick at the emission frequency, we have "radiative-trapping," and the criterion for the critical density must be modified (see Chapter 19).

Note that this definition of $n_{{\rm crit},u}$ depends on the intensity of ambient radiation at frequencies where level u can radiate. For many transitions of interest, we have $(\bar{n}_\gamma)_{u\ell} \ll 1$, and this correction is unimportant, but for radio frequency transitions – e.g., the 21-cm line of atomic hydrogen – it is important to include this correction for stimulated emission.

Critical densities $n_{\rm crit}$ for the fine structure levels of C I, C II, O I, Si I, and Si II are given in Table 17.1.

17.3 Example: H I Spin Temperature

Consider the ground state of the hydrogen atom (electron in the $1s$ orbital, electron spin antiparallel to nuclear spin, $g_0 = 1$), and the hyperfine excited state ($1s$ orbital, electron spin and nuclear spin parallel, $g_1 = 3$). The energy level structure is illustrated in Fig. 17.1.

The energy difference between the excited state (nuclear and electron spins parallel, $g_1 = 3$) and the ground state (nuclear and electron spins antiparallel) is only $E_{10} = 5.87\,\mu{\rm eV}$, corresponding to a photon wavelength $\lambda = 21.11\,{\rm cm}$. The spontaneous decay rate is $A_{10} = 2.884 \times 10^{-15}\,{\rm s}^{-1}$, corresponding to a lifetime of $\sim 10^7\,{\rm yr}$.

[1]The definition of critical density is not completely standard. Some authors include collisional excitation channels in the denominator of Eq. (17.7).

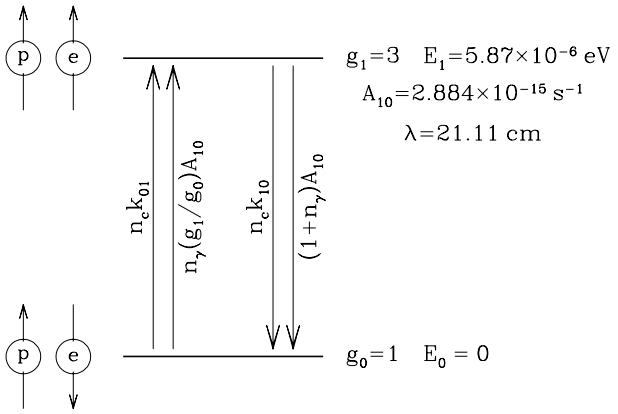

Figure 17.1 Hyperfine splitting of the $1s$ level of H.

The rate coefficient for collisional dexcitation of the hyperfine excited state due to collisions with other H atoms (Allison & Dalgarno 1969; Zygelman 2005) can be approximated by

$$k_{10} \approx \begin{cases} 1.19\times10^{-10} T_2^{0.74-0.20\ln T_2}\,\mathrm{cm^3\,s^{-1}} & (20\,\mathrm{K} < T < 300\,\mathrm{K}) \\ 2.24\times10^{-10} T_2^{0.207} \mathrm{e}^{-0.876/T_2}\,\mathrm{cm^3\,s^{-1}} & (300\,\mathrm{K} < T < 10^3\,\mathrm{K}) \end{cases} . \quad (17.8)$$

We obtain k_{01} from the principle of detailed balance (3.21):

$$k_{01} = 3k_{10}\,\mathrm{e}^{-0.0682\,\mathrm{K}/T} \quad . \quad (17.9)$$

What is the value of the photon occupation number $\bar{n}_\gamma$ in the diffuse ISM? The radiation field near 21 cm is dominated by the cosmic microwave background (CMB) plus Galactic synchrotron emission. Including the contribution[2] from synchrotron radiation, the angle-averaged background near 21 cm corresponds to an antenna temperature $T_A \approx T_{\rm CMB} + 1.04\,\mathrm{K}$ (see Chapter 12), where $T_{\rm CMB} = 2.73\,\mathrm{K}$. Thus

$$\bar{n}_\gamma \equiv \frac{1}{\exp(h\nu/kT_B) - 1} \quad (17.10)$$

$$\equiv \frac{kT_A}{h\nu} \approx \frac{3.77\,\mathrm{K}}{0.0682\,\mathrm{K}} \approx 55 \quad . \quad (17.11)$$

For the present case of a two-level system,

$$n_{\rm crit}(\mathrm{H}) \equiv \frac{(1+\bar{n}_\gamma)A_{10}}{k_{10}} \quad (17.12)$$

$$= 1.7\times10^{-3}(T/100\,\mathrm{K})^{-0.66}\,\mathrm{cm^{-3}} \;\; (50\,\mathrm{K} \lesssim T \lesssim 200\,\mathrm{K}). \quad (17.13)$$

[2]Near 21 cm, even the CMB is in the Rayleigh-Jeans limit, so the antenna temperature T_A and brightness temperature T_B are approximately equal.

where we have taken $\bar{n}_\gamma = 55$, appropriate for H I in the diffuse interstellar medium. In the absence of collisions, the CMB plus Galactic synchrotron radiation would give optically thin H I an excitation temperature $T_{\rm exc} \approx 3.77\,{\rm K}$. If we consider only collisions with atomic H, we can solve Eq. (17.6) for various gas densities $n_{\rm H}$ and temperatures T. Figure 17.2 shows the resulting "spin temperature" $T_{\rm spin} \equiv 0.0682\,{\rm K}/\ln(n_0 g_1/n_1 g_0)$ as a function of density $n_{\rm H}$.

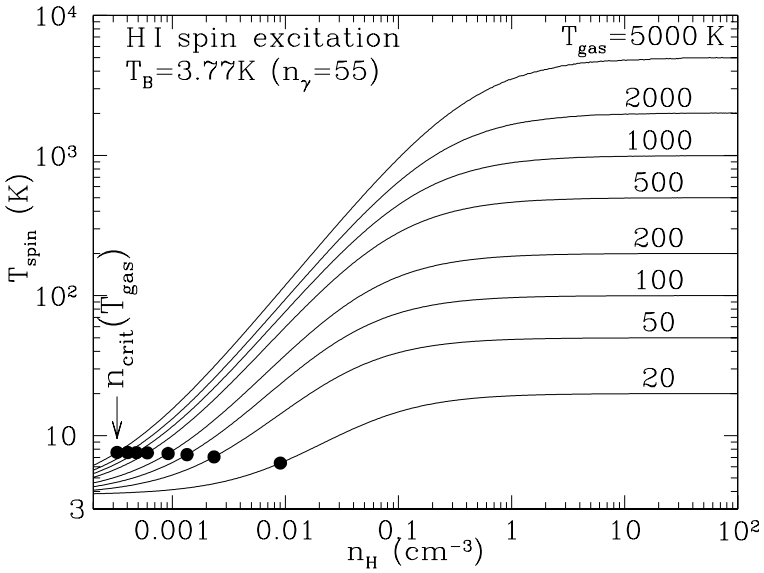

Figure 17.2 H I spin temperature as a function of density $n_{\rm H}$, including only 21 cm continuum radiation (with brightness temperature $T_B = 3.77\,{\rm K}$, i.e., $n_\gamma = 55$) and collisions with H atoms. Lyman α scattering is not included. Filled circles show $n_{\rm crit}$ for each curve.

For densities $n \gg n_{\rm crit}$, we expect $T_{\rm spin} \approx T_{\rm gas}$, while for densities $n \ll n_{\rm crit}$, we expect $T_{\rm spin} \approx T_B(\nu)$, or 3.77K for the radiation field assumed here. The results in Fig. 17.2 are consistent with the expected asymptotic behavior, but it is important to note that one requires $n \gg n_{\rm crit}$ in order to have $T_{\rm spin}$ within, say, 10% of $T_{\rm gas}$, particularly at high temperatures. The points in Figure 17.2 show $n_{\rm crit}(T_{\rm gas})$ for each $T_{\rm gas}$; it is apparent that high values of $T_{\rm spin}$ are achieved only for $n \gg n_{\rm crit}$.

Collisions with protons and electrons can also be important for hyperfine excitation of H I; the rate coefficient for deexcitation by electrons is (Furlanetto & Furlanetto 2007)

$$k_{10}(e^-) \approx 2.26 \times 10^{-9} (T/100\,{\rm K})^{0.5}\,{\rm cm^3\,s^{-1}} \quad (1 \lesssim T \lesssim 500\,{\rm K}), \qquad (17.14)$$

a factor ~ 10 larger than $k_{10}({\rm H})$; electrons will, therefore, be of minor importance

in regions of fractional ionization $x_e \lesssim 0.03$, such as the CNM or WNM (see Figs. 16.1 and 16.2).

Resonant scattering of Lyman-α photons can also change the populations of the hyperfine levels (Wouthuysen 1952; Field 1958).[3] Let P_{01} be the probability per unit time of a transition from the hyperfine ground state to $2p$, followed by spontaneous decay from $2p$ to the hyperfine excited state, and P_{10} the probability per time of a transition from the hyperfine excited state to $2p$, followed by decay to the hyperfine ground state. The Lyman α profile depends on the kinetic temperature of the hydrogen atoms that are emitting and scattering the Lyman α. If the hydrogen atoms have a Maxwellian velocity distribution, Field (1959) showed that $P_{01} \approx 3P_{10}\mathrm{e}^{-0.0682\,\mathrm{K}/T_\mathrm{H}}$, where $T_\mathrm{H} \equiv m_\mathrm{H}\sigma_V^2/k$, and σ_V is the one-dimensional velocity dispersion of the H atoms that are scattering the Lyman α photons. Therefore, this process acts essentially like a collisional process, except that the temperature T_H characterizing the Lyman α line profile includes a contribution from turbulent motions, in addition to microscopic thermal motions. Liszt (2001) estimates the Lyman α intensities expected in the warm neutral medium (WNM), and concludes that collisions and Lyman α together are not fast enough to thermalize the H I hyperfine transition. As a result, we should expect $T_\mathrm{spin} < T_\mathrm{gas}$ in the WNM.

17.4 Example: C II Fine Structure Excitation

The ground electronic state $1s^2 2s^2 2p\ {}^2\mathrm{P}^\mathrm{o}$ of C II contains two fine-structure levels (see Fig. 17.3), ${}^2\mathrm{P}^\mathrm{o}_{1/2}$ and ${}^2\mathrm{P}^\mathrm{o}_{3/2}$. Will the populations of these two levels be thermalized in the ISM? Radiative decay of the ${}^2\mathrm{P}^\mathrm{o}_{3/2}$ excited fine-structure state produces a photon with $\lambda = 158\,\mu\mathrm{m}$. At this wavelength, the continuum background in the interstellar medium has $n_\gamma \ll 1$. In fact, from Figure 12.1, we estimate $n_\gamma \approx 10^{-5}$ in the diffuse ISM. Hence, if we are considering regions that are optically thin in the $158\,\mu\mathrm{m}$ line, we can neglect stimulated emission.

The ${}^2\mathrm{P}^\mathrm{o}_{3/2}$ fine-structure level can be excited by collisions of ${}^2\mathrm{P}^\mathrm{o}_{1/2}$ with electrons, H, He, and (in a molecular cloud) H_2. For electrons, the collision strength is (Keenan et al. 1986)

$$\Omega({}^2\mathrm{P}^\mathrm{o}_{1/2}, {}^2\mathrm{P}^\mathrm{o}_{3/2}) \approx 2.1 \quad , \tag{17.15}$$

[3] The Wouthuysen-Field effect can be understood semiclassically. When a Lyman α photon is absorbed, the H atom enters a $2p$ state with its electronic angular momentum $\mathbf{L}$ in some direction that is related to the direction of propagation and polarization of the absorbed photon, but is unrelated to the orientation of the nuclear or electron spins. During the $\sim 10^{-9}$ s lifetime of the ${}^2\mathrm{P}^\mathrm{o}_{1/2}$ or ${}^2\mathrm{P}^\mathrm{o}_{3/2}$ excited state, spin-orbit coupling will cause both the electron spin $\mathbf{S}$ and orbital angular momentum $\mathbf{L}$ to precess around $\mathbf{L} + \mathbf{S}$. When the Lyman α photon is emitted, the electron spin will be in a different direction, and thus its orientation relative to the nuclear spin will change some fraction of the time. Note that while the spin-orbit coupling in H is weak, it is not zero: the $0.366\,\mathrm{cm}^{-1}$ fine-structure splitting between ${}^2\mathrm{P}^\mathrm{o}_{3/2}$ and ${}^2\mathrm{P}^\mathrm{o}_{1/2}$ corresponds to an electron precession frequency $\sim 8 \times 10^{10}$ Hz – the ~ 1.6 ns lifetime of the excited state corresponds to $\sim 10^2$ precession periods.

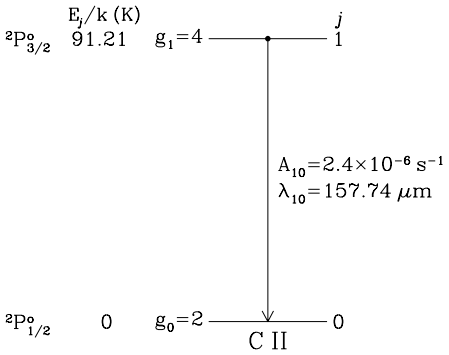

Figure 17.3 Fine-structure levels of C^+.

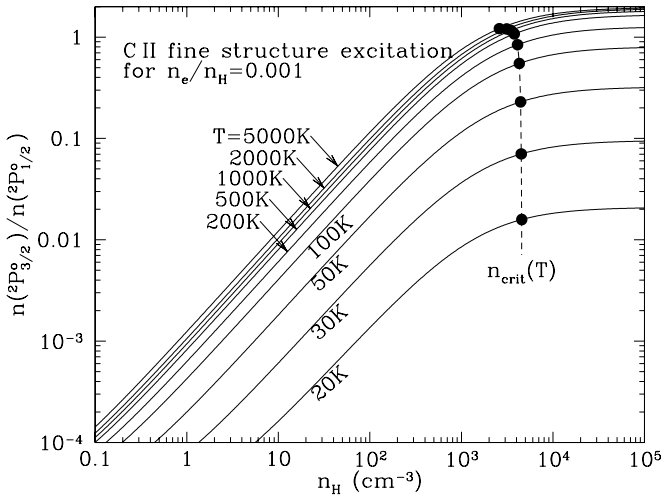

Figure 17.4 Excitation of the $^2P^o_{3/2}$ excited fine-structure level of C^+. The background radiation is assumed to have $n_\gamma \approx 10^{-5}$ at $158\,\mu$m.

so that

$$k_{10}(e^-) \approx 4.53 \times 10^{-8} T_4^{-1/2}\,\mathrm{cm^3\,s^{-1}} \quad , \tag{17.16}$$

while for H atoms (Barinovs et al. 2005):

$$k_{10}(\mathrm{H}) \approx 7.58 \times 10^{-10} T_2^{0.1281+0.0087\ln T_2}\,\mathrm{cm^3\,s^{-1}} \quad . \tag{17.17}$$

Thus the critical densities are

$$n_{\rm crit}({\rm H}) \approx 3.2 \times 10^3 T_2^{-0.1281-0.0087 \ln T_2}\,{\rm cm}^{-3} \quad , \tag{17.18}$$

$$n_{\rm crit}(e^-) \approx 53\, T_4^{1/2}\,{\rm cm}^{-3} \quad . \tag{17.19}$$

Therefore, we see that for both CNM and WNM conditions, the densities are well below critical, and the C II fine-structure levels will be subthermally excited. It follows that collisional excitations of C II $^2{\rm P}^{\rm o}_{3/2}$ will usually be followed by radiative decays, removing energy from the gas. The [C II] 158 μm transition is the principal cooling transition for the diffuse gas in star-forming galaxies. Plate 3c is an all-sky map of [C II] 158 μm emission from the Galaxy, made by the Far InfraRed Absolute Spectrophotometer (FIRAS) on the COsmic Background Explorer (COBE) satellite (Fixsen et al. 1999).

The preceding discussion neglects radiative excitation of C II $^2{\rm P}^{\rm o}_{3/2}$, appropriate for clouds that are optically thin in the [C II] 158 μm line. When the clouds become optically thick, the [C II] 158 μm line intensity can increase to the point where self-absorption makes an important contribution to the excitation of C II $^2{\rm P}^{\rm o}_{3/2}$. We will return to the question of excitation under such conditions in Chapter 19.

17.5⋆ Three-Level Atom

If we consider the ground state and two excited states, we refer to this as a "three-level atom." The equations for the evolution of the level populations are

$$\frac{dn_2}{dt} = R_{02} n_0 + R_{12} n_1 - (R_{20} + R_{21})\, n_2 \quad , \tag{17.20}$$

$$\frac{dn_1}{dt} = R_{01} n_0 + R_{21} n_2 - (R_{10} + R_{12})\, n_1 \quad , \tag{17.21}$$

where the rates R_{if} are:

$$R_{10} = C_{10} + (1 + n_{\gamma,10}) A_{10} \quad , \tag{17.22}$$

$$R_{20} = C_{20} + (1 + n_{\gamma,20}) A_{20} \quad , \tag{17.23}$$

$$R_{21} = C_{21} + (1 + n_{\gamma,21}) A_{21} \quad , \tag{17.24}$$

$$R_{01} = (g_1/g_0) \left[C_{10} {\rm e}^{-E_{10}/kT} + n_{\gamma,10} A_{10} \right] \quad , \tag{17.25}$$

$$R_{02} = (g_2/g_0) \left[C_{20} {\rm e}^{-E_{20}/kT} + n_{\gamma,20} A_{20} \right] \quad , \tag{17.26}$$

$$R_{12} = (g_2/g_1) \left[C_{21} {\rm e}^{-E_{21}/kT} + (g_2/g_1) n_{\gamma,21} A_{21} \right] \quad . \tag{17.27}$$

The rates $C_{u\ell}$ for collisional deexcitation are summed over all collision partners c:

$$C_{u\ell} \equiv \sum_c n_c k_{u\ell}(c) \quad , \tag{17.28}$$

and we assume each colliding species to have a thermal velocity distribution corresponding to temperature T. For the three-level system, the solution is tractable:

$$\frac{n_1}{n_0} = \frac{R_{01}R_{20} + R_{01}R_{21} + R_{21}R_{02}}{R_{10}R_{20} + R_{10}R_{21} + R_{12}R_{20}} \quad , \tag{17.29}$$

$$\frac{n_2}{n_0} = \frac{R_{02}R_{10} + R_{02}R_{12} + R_{12}R_{01}}{R_{10}R_{20} + R_{10}R_{21} + R_{12}R_{20}} \quad . \tag{17.30}$$

For systems with more than three energy levels, the steady state level populations are usually found using numerical methods to solve the system of linear equations.

17.6⋆ Example: Fine Structure Excitation of C I and O I

C I ($1s^2 2s^2 2p^2$) and O I ($1s^2 2s^2 2p^4$) are two important examples of atoms with triplet ($S = 1$) ground states (see Fig. 17.5). Using collisional rate coefficients from Appendix F, we can solve for excitation of these levels. Results for n_1/n_0 for C I are shown in Fig. 17.6, and n_1/n_0 for O I are shown in Fig. 17.7. For both cases, we have assumed a fractional ionization $n_e/n_{\rm H} = 10^{-3}$ characteristic of H I clouds or photodissociation regions.

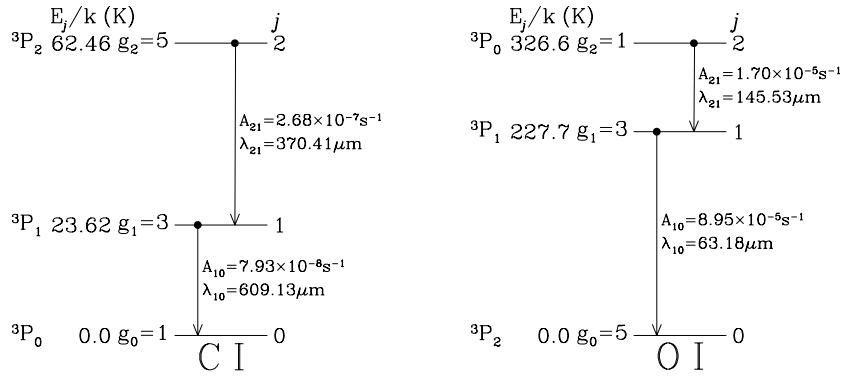

Figure 17.5 Fine-structure levels of C I and O I.

17.7⋆ Measurement of Density and Pressure Using C I

The fine-structure excited states of C I, with energies $E_1/k = 23.6\,{\rm K}$ and $E_2/k = 62.5\,{\rm K}$, can be collisionally populated even at low temperatures, and the level populations can be measured using C I's rich spectrum of ultraviolet absorption lines

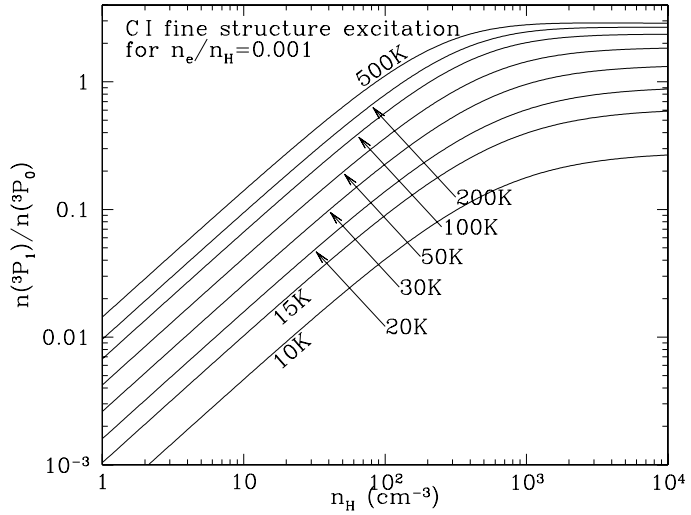

Figure 17.6 Excitation of C I $^3P_1$, source of 609.1 μm emission.

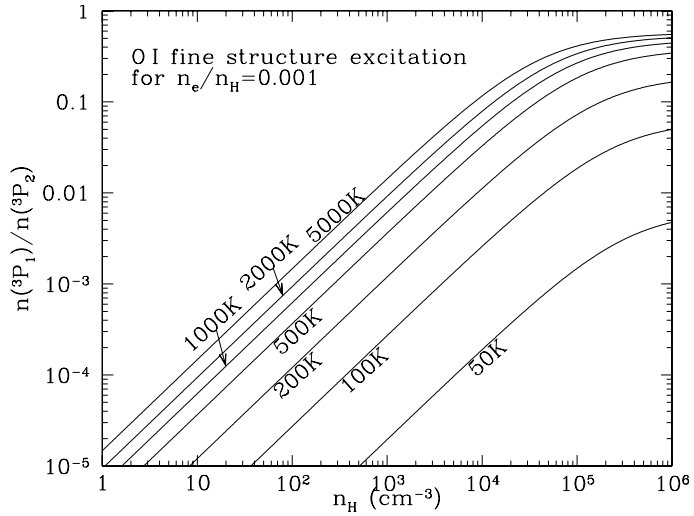

Figure 17.7 Excitation of O I $^3P_1$, source of 63.18 μm emission.

(see Appendix E). Because the critical density $n_{\rm H,crit}$ (see Table 17.1) is higher than the densities in typical diffuse clouds, the population of the C I fine structure levels can be used to constrain the density and temperature (Jenkins & Shaya 1979). A recent study by Jenkins & Tripp (2010) used high-quality spectra of UV absorption lines of C I on 89 sightlines to characterize the distribution of thermal pressures in diffuse clouds.

For a given gas composition (fractional ionization and H_2 fraction), temperature T, and density, the fractions $f_1 \equiv N(^3P_1)/N(\mathrm{C\,I})$ and $f_2 \equiv N(^3P_2)/N(\mathrm{C\,I})$ of

the C I that are in the first and second excited states $^3\mathrm{P}_1$ and $^3\mathrm{P}_2$ of the ground electronic state $^3\mathrm{P}$ can be calculated theoretically (e.g., Fig. 17.6 shows f_1/f_0). For a given T, varying the thermal pressure p will generate a track in the f_1–f_2 plane. Theoretical tracks for $T = 30\,\mathrm{K}$, 80 K, and 300 K are shown in Figure 17.8, with each track generated by varying the pressure from $p/k = 10^2\,\mathrm{cm}^{-3}\,\mathrm{K}$ to $10^7\,\mathrm{cm}^{-3}\,\mathrm{K}$.

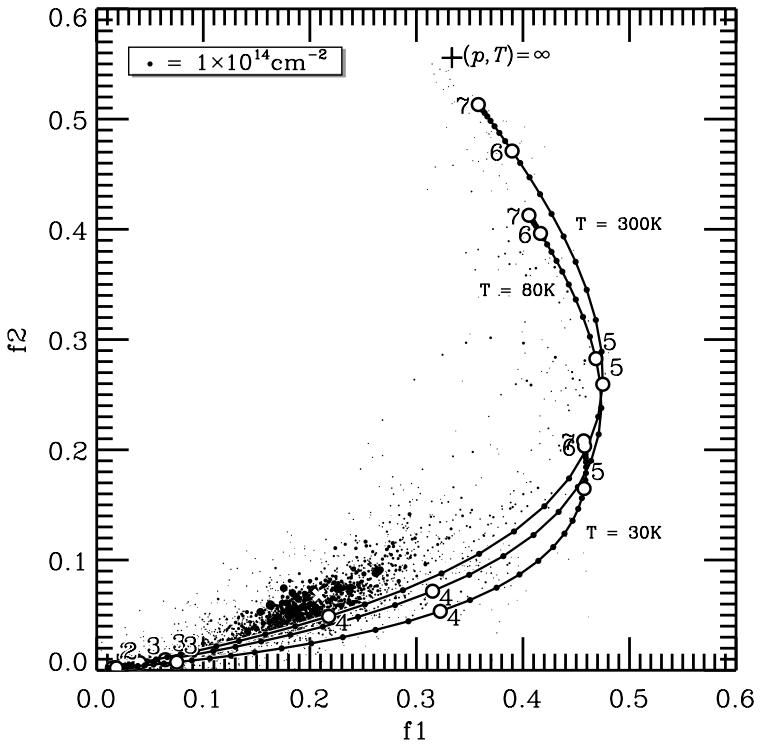

Figure 17.8 $f1$ and $f2$ are the fractions of C I that are in the $^3\mathrm{P}_1$ and $^3\mathrm{P}_2$ excited fine structure states. Solid lines are theoretical tracks for three different temperatures (30 K, 80 K, 300 K), as the pressure is varied from $p/k = 10^2\,\mathrm{cm}^{-3}\,\mathrm{K}$ to $10^7\,\mathrm{cm}^{-3}\,\mathrm{K}$, with numbers indicating the value of $\log_{10}[p/k(\,\mathrm{cm}^{-3}\,\mathrm{K})]$. Data points are measurements for different velocity components on 89 sightlines. The area of each dot is proportional to $N(\mathrm{C\,I})$. The white $\times$ is the "center of mass" value $(f1, f2) = (0.21, 0.068)$. Taken from Jenkins & Tripp (2010).

Observed values of (f_1, f_2) are also plotted in Figure 17.8. Typically $f_1 \approx 0.20$ of the C I is found to be in the $^3\mathrm{P}_1$ level, and $f_2 \approx 0.07$ is in the $^3\mathrm{P}_2$ level, although on some sightlines f_2 can exceed 0.50. Note that the observed values of (f_1, f_2) usually fall somewhat *above and to the left* of the theoretical tracks. Jenkins & Tripp (2010) interpret this tendency as resulting from superposition of two components: a dominant component with moderate pressure p plus a small

amount of high-pressure material.[4] UV pumping can also populate the excited fine-structure levels, and Jenkins & Tripp (2010) correct for this in their estimates for p.

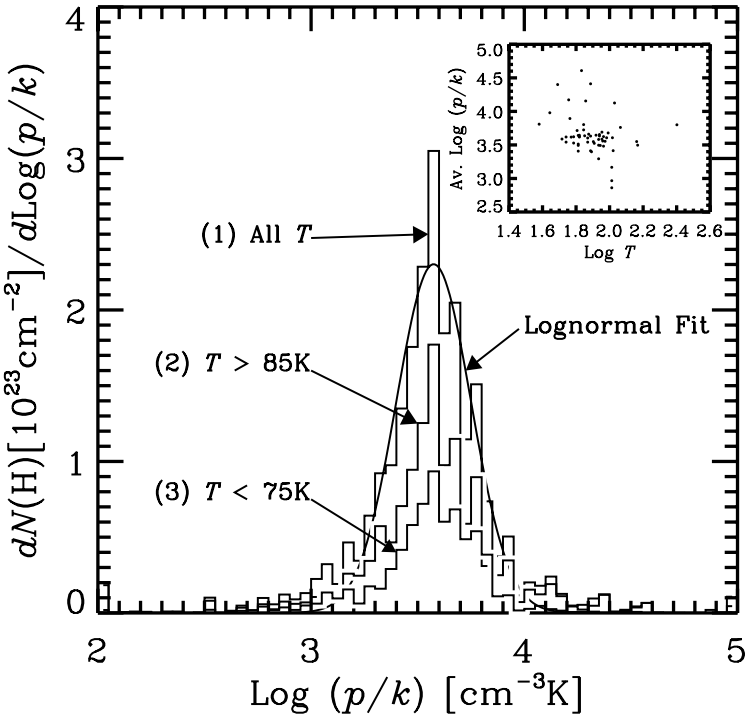

Figure 17.9 Distribution of thermal pressures measured using C I absorption lines (see text). Taken from Jenkins & Tripp (2010).

The distribution of pressures found by Jenkins & Tripp (2010) is shown in Fig. 17.9. The observed distribution can be approximated by a log-normal distribution with a peak at $p/k \approx 10^{3.575}\,\mathrm{cm}^{-3}\,\mathrm{K} \approx 3800\,\mathrm{cm}^{-3}\,\mathrm{K}$.

In many cases it was possible to determine the gas temperature using the H_2 $J = 1 - 0$ rotation temperature $T_{\rm rot}$. The inset in Fig. 17.9 shows the distribution of p and $T_{\rm rot}$; there appears to be no correlation between $T_{\rm rot}$ and p. For the "typical" $p/k \approx 3800\,\mathrm{cm}^{-3}\,\mathrm{K}$, the H_2 rotation temperatures range from $\sim 50\,\mathrm{K}$ to $\sim 250\,\mathrm{K}$.

Jenkins & Tripp (2010) conclude that interstellar clouds routinely contain a small amount of gas that is at the same bulk velocity but at a pressure that is much higher than the average pressure in the cloud – this is the only way that they can explain the tendency of the data points in Fig. 17.8 to fall above and to the left of the theoretical tracks. This is a very surprising result, as there is no obvious explanation for

[4] Jenkins & Tripp (2010) assume the high-pressure material to have $(f_1, f_2) = (0.38, 0.50)$.

why a small fraction of the cloud material should be overpressured without being at a significantly different velocity. It may be conjectured that the overpressured regions are the result of highly localized intermittent heating, perhaps due to turbulent dissipation, but the situation remains unclear. It is at least conceivable that the problem could be with the collisional rate coefficients – if, for example, the current theoretical rates have too small a value of C_{20}/C_{10}, then the true tracks at the low-pressure end of Fig. 17.8 would have a larger slope, perhaps passing through the cloud of points near (0.2,0.06) in Fig. 17.8, and removing the need to invoke an admixture of high pressure material.